CHINA FOUNDRY Research & Development
Vol. 23 No. 2 March 2026
www.springer.com/41230
https://doi.org/10.1007/s41230-026-5097-2

Creep behavior and fracture mechanism of high Al/Nb-containing TiAl alloy

Yan Wang, *Qi Wang, **Rui-run Chen, Yan-qing Su, and Heng-zhi Fu

National Key Laboratory for Precision Hot Processing of Metals, School of Materials Science and Engineering, Harbin Institute of Technology, Harbin 150001, China

Abstract: High Al content inhibits the formation of B2 phase, which improves creep resistance in high Al/Nb-containing TiAl alloys. In this work, the microstructure evolution and creep behavior of TiAl based alloy Ti-46Al-8Nb (at.%) with a high Al/Nb content, produced by the vacuum consumable electrode melting technology and the electromagnetic cold crucible melting technology, were studied. The microstructure of the Ti-46Al-8Nb alloy is composed of α_2/γ phases arranged in layers with different orientations, which possesses smooth grain boundaries due to small-blocky segregation and irregular serrated grain boundaries caused by large-blocky segregation. Under conditions of 780–820 °C and 125–175 MPa for 200 h, it exhibits typical power-law creep characteristics. The apparent activation energy of creep (Q) and apparent stress exponent (n) of the Ti-46Al-8Nb alloy are Q=274 kJ·mol^{-1} and n=1.97, respectively. The creep deformation mechanism is grain boundary sliding. Cracks easily form at the smooth boundary. The irregular serrated boundaries with small specific surface area hinder the dislocation movement, thereby improving the boundary creep resistance. When the stress concentration reaches a certain degree, the cracks will initiate between the lamellar structures within the grain. The crack usually propagates along the boundary perpendicular to or at an angle of 45° with the stress axis until creep failure occurs.

Keywords: high Al/Nb TiAl alloy; cold crucible solidification; microstructure; creep behavior

CLC numbers: TG146.23 **Document code:** A **Article ID:** 1672-6421(2026)02-274-09

1 Introduction

Due to the long-term operation of aero-engine components under high-temperature and high-pressure conditions, increasing stringent requirements are proposed on the high temperature performance of materials. The advanced intermetallic TiAl-based alloy is considered the most promising in terms of development high-temperature structural material in the aerospace industry field by reason of its outstanding overall mechanical properties[1-3], such as low density, high specific strength, and outstanding oxidation resistance[4-6]. So far, with the unremitting efforts of scientists, some systems of TiAl-based alloys have been successfully applied to low-pressure turbine blades in aero-engines[7,8]. However, the insufficient creep resistance and poor room temperature plasticity of TiAl-based alloys hinder their widespread applications[2]. Adding high melting point elements such as Nb to the alloy system is an effective method to improve the high-temperature performance of TiAl-based alloys. The rapid development of high-Nb TiAl-based alloy has become the possibility to solve the problem of its limited applications[9], with the ultimate service temperature being 60–100 °C higher than that of traditional TiAl alloy[10-12].

In addition, it has been reported that the creep properties of TiAl-based alloys are quite susceptible for the change of microstructure[13-15]. In general, the full lamellar (FL) and near lamellar (NL) structures have good high-temperature creep resistance. Through heat treatment[16], directional solidification[6], thermal mechanical processing[17], and other methods, the microstructure of the alloy can be controlled to improve the creep resistance. With the introduction of high-melting point elements, the requirements for alloy

*Qi Wang

Ph. D., Associate Professor. He has been selected for the National Young Talent Program. He has published over 110 SCI papers and has applied for and obtained more than 70 patents. His research mainly focuses on melting and solidification of high-temperature materials.

E-mail: wangqi_hit@hit.edu.cn

**Rui-run Chen

E-mail: ruirunchen@hit.edu.cn

Received: 2025-04-27; Revised: 2025-10-09; Accepted: 2025-11-24

melting are higher. Electromagnetic cold crucible melting technology has been widely used in the melting and preparation of materials because of its advantages of melting high-melting point, active materials and uniform composition of prepared materials. Electromagnetic cold crucible technology is often used to prepare high-temperature active metals such as Ti-based alloys[18], TiAl-based alloys[19-21], and monocrystalline silicon[22,23] by melting. Therefore, in this work, a fully lamellar high-Nb TiAl alloy was prepared using electromagnetic cold crucible solidification technology to obtain good creep resistance.

Most of metals or alloys have the similar creep characteristics, including initial-creep stage, steady-creep stage, and accelerated-creep stage[24]. The steady-creep stage of the alloy, balanced by the mutual restriction of work hardening and dynamic recovery, is of great significance for inferring the creep mechanism. Just at this moment, the creep rate is the smallest and constant. The apparent stress exponent of creep can be calculated by the minimum creep rate in the steady-state stage, which can be used to infer the creep mechanism[25]. Therefore, a creep test with a duration of 200 h was carried out to obtain the steady-state creep rate for calculation.

The microstructure of TiAl-based alloy is quite sensitive to changes in Al content[26]. The content of B2 phase will gradually decrease with the increase of Al content, because the increase of Al element changes the solidification path, thereby affecting the formation of B2 phase. Liang et al.[27] found that as the content of Al element increased, the solidification path changed from single β solidification to a mixed form of β solidification and interdendritic peritectic solidification, limiting the formation of B2 phase and improving the creep resistance. Previous research[28-30] on high-Nb TiAl alloys mainly focused on Al content ranging from 43at.% to 45at.%, while, in this study, a TiAl-based alloy with a nominal composition of 46at.% was used.

An electromagnetic cold crucible was utilized to prepared Ti-46Al-8Nb alloy with a fully lamellar structure. The creep behavior was systematically studied under temperature and stress conditions close to the actual working environment. The correlation between microstructure and properties was established, and the creep mechanism at a given temperature and stress level was clarified to assist in the safety design of TiAl-based alloys in practical situations.

2 Materials and methods

2.1 Material preparation

The raw materials for melting were pure titanium (99.99wt.%), high-purity aluminum (99.97wt.%), and Al-Nb alloys. The materials used in this work were repeatedly melted three times using vacuum consumable electrode melting under a vacuum degree not exceeding 1.3×10^{-1} Pa and a leakage rate not exceeding 0.10 Pa·min^{-1}. Then, they were remelted via electromagnetic cold crucible melting to reduce cracks to obtain a 15 kg ingot. The ingot was cut into the specimens with cross-section of 4 mm×2 mm and a gauge length of 24 mm for creep testing. The nominal composition (in at.%) of the alloy in this study was Ti-46Al-8Nb. The actual alloy composition (in at.%) was detected using inductively coupled plasma atomic emission spectroscopy (ICP-AES) technology. Table 1 summarizes its actual chemical compositions.

Table 1: Chemical composition of Ti-46Al-8Nb alloy (at.%)

Nominal composition	Experimental composition		
Ti-46Al-8Nb	Ti	Al	Nb
	46.74	45.39	7.87

2.2 Microstructure characterization

Microstructure before and after creep was characterized using optical microscopy (OM, Olympus, GX-71, China) and scanning electron microscopy (SEM, Hitachi, TM4000, Japan) in back scattered electron (BSE) mode. The samples used for microstructure observation were processed by sanding with 400, 800, 1200, 2000 mesh standard SiC abrasive papers, mechanical polishing with diamond paste (W1.5), and etching in an optimized Kroll reagent of 20% HF, 2% HNO_3, and 78% H_2O (vol.%) for 4–5 s. The phase constitution was assessed by X-ray diffractometer (XRD, Panalytical, Empyrean, Netherlands) with Cu-Kα radiation scanning from 20°–90° at a scanning speed of 10°·min^{-1}.

2.3 Creep performance characterization

Figure 1 shows the device, sample size, and the process of the creep testing. The creep performance testing was carried out using the uniaxial tensile mode of the electronic creep endurance testing machine (LISHI, LDRD-50, China) under vacuum condition to obtain creep curves under conditions of 780, 800, 820 °C and 125, 150, 175 MPa for 200 h, with a constant load loading method, as shown in Fig. 1. The deformation during creep process was measured and recorded by the deformation measurement system and data acquisition system provided by the creep testing machine. Based on the obtained data of creep curves, the apparent stress exponent and the apparent creep active energy were calculated.

3 Results

3.1 As-cast microstructure

The X-ray diffraction pattern of Ti-46Al-8Nb alloy is shown in Fig. 2. Obviously, there are three phases, which are α_2, γ, and B2 phase. Figure 3 shows the as-cast microstructure of the Ti-46Al-8Nb alloy. In the Ti-46Al-8Nb alloy, both α_2 and γ phases mainly present in the form of lamellae, and alternately arrange for forming α_2/γ lamellar colony. Besides, two typical micro-segregations in this alloy, namely, α-segregation and β-segregation are commonly found. When the content of Nb and W in some segregation area inside a phase exceeds ~10at.%, the $\alpha\rightarrow\alpha_2+\beta+\gamma$ transformation may occur during

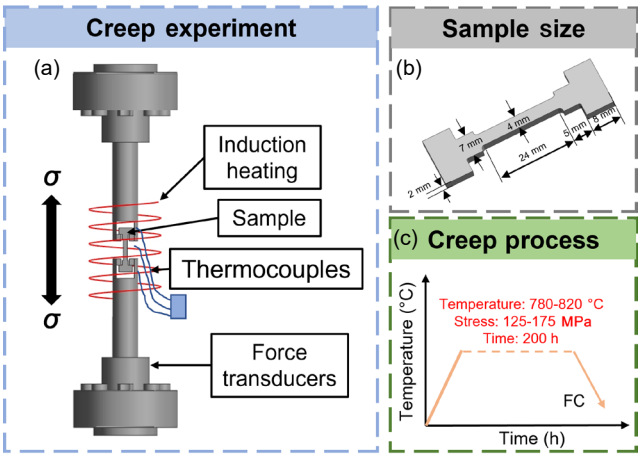

Fig. 1: A schematic diagram about creep experimental device and process: (a) creep experimental device; (b) creep specimen size; (c) creep experiment process

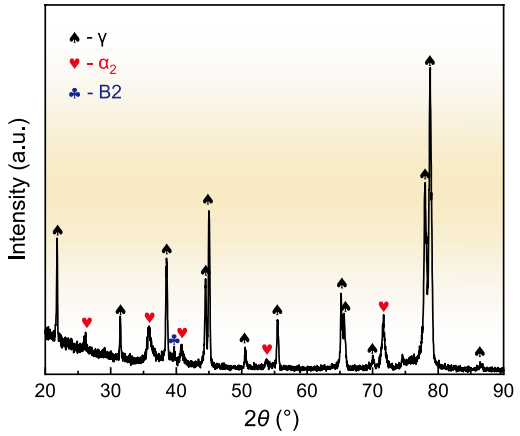

Fig. 2: X-ray diffraction pattern of phase in Ti-46Al-8Nb alloy

cooling, leading to the formation of local lamellar structure of $\alpha \rightarrow \alpha_2+\beta+\gamma$. Because of the phase transition from $\alpha \rightarrow \alpha_2+\beta+\gamma$, a localized lamellar structure consisting of α_2, β, and γ plates is formed, resulting in α-segregation. The reason for β-segregation is that ascribed to the phase transformation of $\beta \rightarrow \alpha$ occurred in the course of the cooling period[31].

The OM microstructure of the Ti-46Al-8Nb alloy is shown in Fig. 3(a). The average size of the lamellar grain is measured to be 264.8 μm by the linear intercept method. The SEM-BSE microstructure of the Ti-46Al-8Nb alloy is shown in Figs. 3(b) and (c), exhibiting many lamellar α_2/γ phase regions in the matrix. In this lamellar microstructure, a region in which the lamellae have the same orientation is regarded as a single grain. Due to different degrees of segregation, there are two types of grain boundary morphology, smooth and irregular, in the boundaries of lamellae structure with different orientations, as the arrow in Fig. 3(b). There are numerous blocky γ and B2 phases present within the grain boundary region. Besides, a handful of blocky γ+B2 phases exist within the grains, as shown in Figs. 3(b) and (c). The formation of blocky γ phases is due to the repulsion of Al element into the inter-dendritic region during the solidification process. Similarly, Nb element, as a β-stabilizer element, has a lower diffusion rate in alloys, which leads to the disordered β phase at high temperatures being retained at room temperature and ordering to form B2 phase[32].

3.2 Creep properties

Figure 4 shows the creep curves of the Ti-46Al-8Nb alloy tested at 780–820 °C and 125–175 MPa for 200 h. Based on curve characteristics, it demonstrates that the application of load is accompanied by the occurrence of initial creep

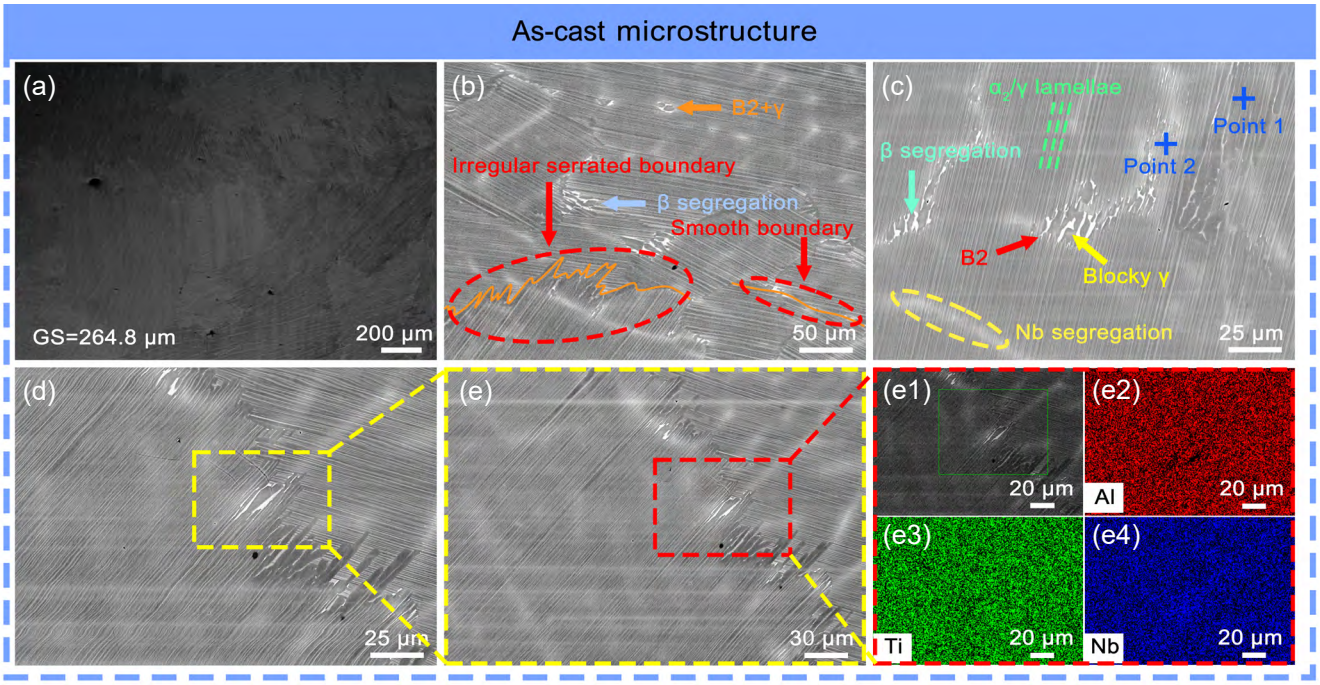

Fig. 3: As-cast microstructure of Ti-46Al-8Nb alloy: (a) OM image; (b–e) SEM image; (e1–e4) EDS mapping

strain. As the creep process progresses, the creep strain rate decreases. The measured curves all exhibit an obvious steady-state creep. Obviously, as the creep temperature and applied stress increase, both creep strain and creep rate increase gradually.

Figure 4(a) shows the creep curves measured at 800 °C under 125–175 MPa conditions for 200 h. The creep resistance of Ti-46Al-8Nb alloy under stress (σ) of 125 MPa is superior to that under other stress conditions, and the strain rate (ε) during the steady-state creep stage is 0.0081%·h^{-1}. At 800 °C, as the applied stress increases from 150 MPa to 175 MPa, the strain rate in the steady-state creep stage increases from 0.0120%·h^{-1} to 0.0156%·h^{-1}.

Figure 4(b) shows the creep curves of the Ti-46Al-8Nb alloy under the stress of 150 MPa at 780–820 °C for 200 h. It shows that the alloy exhibits an excellent creep resistance at 780 °C, and the creep strain rate in the steady-state creep stage is 0.0065%·h^{-1}. The creep strain rate is measured to be 0.0182%·h^{-1} during the steady-state creep stage when the temperature is increased to 820 °C. The summary of creep related parameters measured under different conditions is shown in Fig. 5.

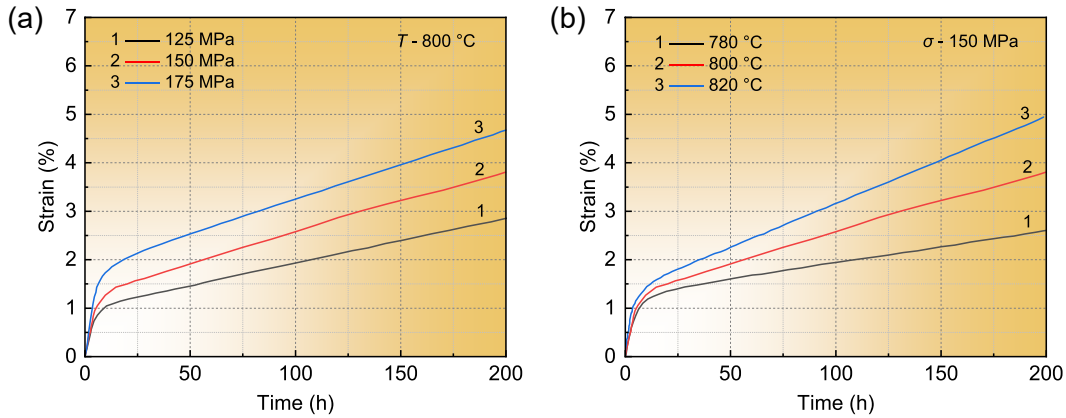

Fig. 4: Creep curves of Ti-46Al-8Nb alloy at different conditions: (a) 800 °C, 125–175 MPa; (b) 780–820 °C, 150 MPa

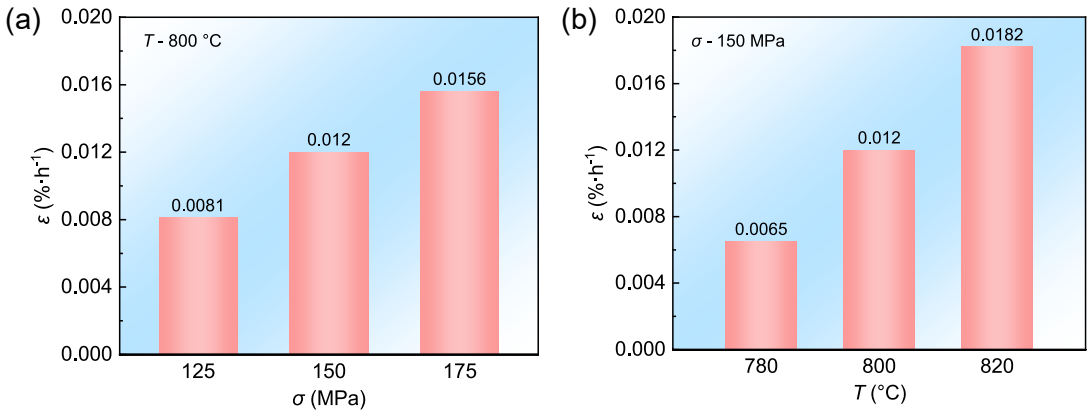

Fig. 5: Steady-state creep strain rate of Ti-46Al-8Nb alloy under different conditions: (a) 800 °C, 125–175 MPa; (b) 780–820 °C, 150 MPa

3.3 Deformed microstructure after creep testing

Figure 6 shows the deformed microstructure of Ti-46Al-8Nb alloy after 200 h of creep test under the 780–820 °C and 125–175 MPa conditions. The specimens subjected to creep under various conditions do not fracture after 200 h. When the creep temperature is 800 °C, as the applied stress gradually increases, the voids in the microstructure gradually increase. Under the stress conditions of 125 MPa, the alloy only has a small number of small-sized voids at grain boundaries and within the grains, as shown in Fig. 6(b). When the stress reaches 175 MPa, the voids in the deformed microstructure grow and connect [Fig. 6(d_1)], and cracks appear [Fig. 6(d_2)]. These voids and cracks mainly exist in grain boundaries and the interface of lamellar within the grains, as shown in Figs. 6(c) and (d_1 and d_2). Similarly, when the applied stress is 150 MPa, as the creep temperature increases, the void size gradually increases, and small voids can be observed at the end of the crack, as shown in Figs. 6(a), (c), and (e). Upon closer observation of Figs. 6(d_1 and d_2) and (e), it can be found that when the morphology of grain boundaries is smooth, cracks will propagate along the grain boundaries. On the contrary, when the grain boundaries are irregularly serrated, there are discontinuous voids at the grain boundaries, and cracks will develop along interlayer within the grains. The crack propagation direction in the alloy is perpendicular or approximately 45° to the stress axis.

Based on the above experimental results, the voids mainly nucleate at the grain boundaries and the positions of B2 phase

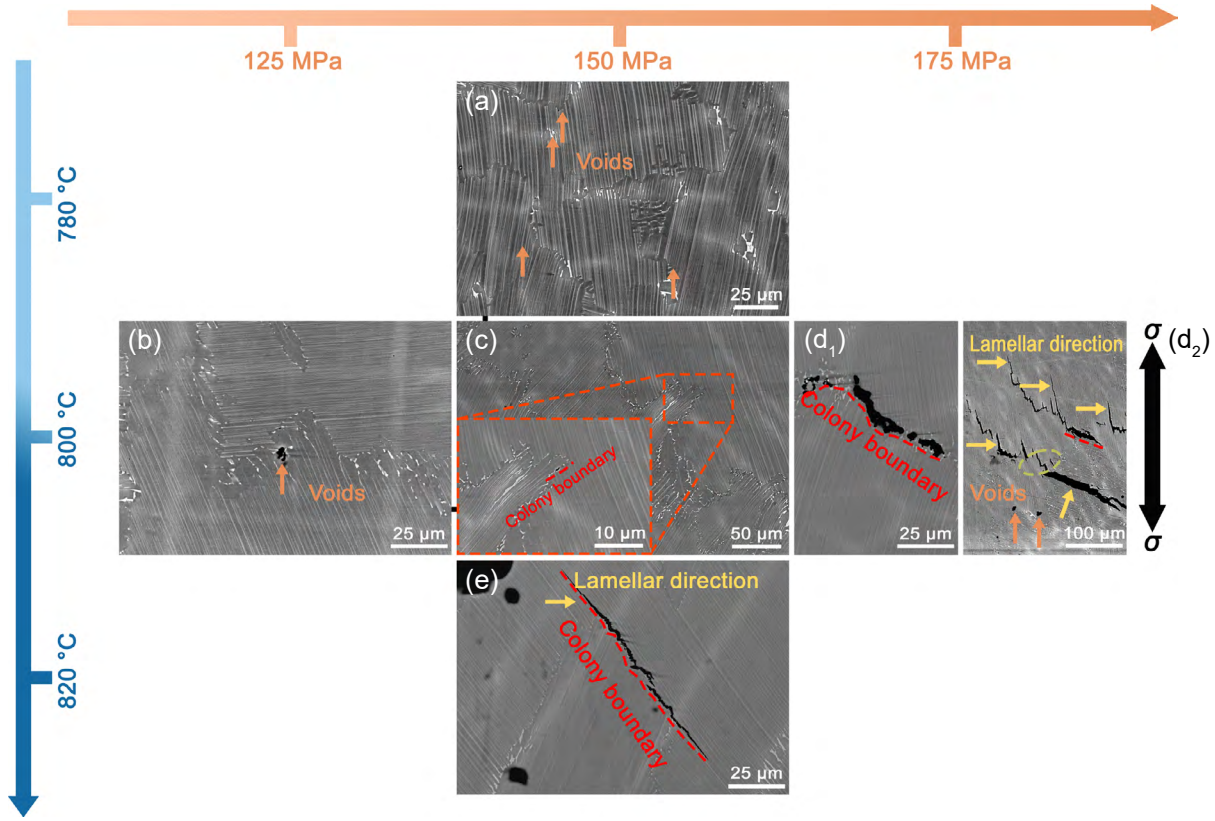

Fig. 6: SEM-BSE microstructure of alloy after creep test at 780–820 °C and 125–175 MPa for 200 h: (a) 780 °C/150 MPa; (b) 800 °C/125 MPa; (c) 800 °C/150 MPa; (d) 800 °C/175 MPa; (e) 820 °C/150 MPa

within the grains, which is caused by the incompatibility between B2 phase and the other surrounding phases during the deformation process. In addition, the reason why cracks propagate in the direction perpendicular to or at a 45° to the stress axis is that the shear stress in that direction is higher.

In general, smooth grain boundaries contribute to crack propagation[33]. Voids and cracks in the alloy are more likely to form at grain boundaries with segregation. This is the result of the combined effect of stress concentration caused by the segregation and strain incompatibility between its surrounding phases during deformation, as well as lower interfacial bonding strength between different phases. The cavities at the grain boundaries are interconnected, promoting the propagation of cracks along the grain boundaries, thereby releasing stress concentration and accelerating creep failure.

Irregular grain boundaries can suppress crack growth and propagation[34]. Discontinuous cracks are formed at irregular grain boundaries in alloy specimens after creep. This is due to the strengthening effect of grain boundary formed by bulk segregation at the grain boundary, which can enhance the slip resistance of the grain boundary and prevent the initiation and propagation of cracks. Therefore, cracks propagate along the layered interface to release stress concentration until creep failure occurs.

4 Discussion

4.1 Effect of Al content on microstructure

The content of Al element plays a decisive role in the microstructure of TiAl alloy. In binary alloy systems, solidification pathways are divided into three typical types based on the different Al contents[35]: (1) Al<44.8at.%, the solidification pathway is single β solidification; (2) 44.8at.%<Al<47.3at.%, the solidification pathway is hypo-peritectic solidification; (3) Al>49.4at.%, the solidification pathway is hyper-peritectic solidification. The introduction of β-stabilizing elements has an impact on the solidification path[36]. Therefore, the concept of "Al equivalent" is introduced to more accurately determine the solidification path. The Al equivalent can be expressed by the following equation[37]:

$$C_{Al,eq} = C_{Al} - (C_a X_a + C_b X_b + C_c X_c) \quad (1)$$

where $C_{Al,eq}$ is the Al equivalent; C_{Al} is the Al content; C_x is the content of x elements in the alloy system; X_x is the Al equivalents for element x. Previous studies have shown that X_{Nb} changes with the Nb content. For Ti-46Al-8Nb alloy, X_{Nb}=+0.18[38]. According to the black contrast in Fig. 3(c) and Table 2, Al element is repelled to the interdendritic region at the same time as the formation of primary dendrite β phase during the actual solidification process. Therefore, the actual Al equivalent calculation result is 46.23at.%. It means that the solidification pathway of the alloy involves more complex hypo-peritectic solidification, as shown in Fig. 7.

When the alloy solidifies to a certain temperature, the primary β phase undergoes a constant temperature transformation with the residual liquid phase, thereby promoting the growth of the peritectoid phase [see α_h in Fig. 7(c)]. The β phase at high temperatures is consumed during this process. Compared to

Table 2: Chemical composition of different points in Fig. 3(c) (at.%)

Point	Ti	Al	Nb
1	45.02	47.67	7.31
2	45.74	45.39	8.87

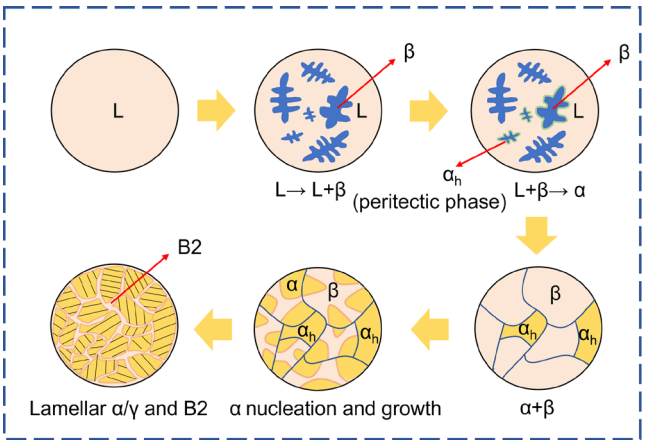

Fig. 7: Schematic of solidification pathway of Ti-46Al-8Nb alloys

the single β solidification, the content of B2 phase formed by the disordered β phase maintaining and undergoing ordering at room temperature also decreases accordingly. Previous studies[39] have shown that the B2 phase deteriorates the properties of alloys due to strain incompatibility with other phases. In general, increasing the Al content of the alloy will suppress the formation of B2 phase in the alloy, weaken the instability of the structure, and improve the creep resistance of the alloy.

4.2 Related parameters and constitutive equation of creep

The creep mechanism of TiAl-based alloy is usually discussed based on the steady-state creep stage[40]. The creep strain rate at steady-state is the result of the competition between work hardening and dynamic recovery. Work hardening causes the energy inside the alloy to continue to rise due to the activation of a large amount of dislocations for sliding. The energy drives dynamic recovery, that is, defect elimination and the reconstruction of dislocations that form small angle grain boundaries. When work hardening and dynamic recovery reach equilibrium over a large strain span, the alloy exhibits steady-state creep. The steady-state or minimum creep strain rate is generally described by Dorn law[41-42]:

$$\varepsilon = A\sigma_A^n \exp\left(-\frac{Q}{RT}\right) \quad (2)$$

where ε is the creep strain rate in the steady-state creep stage; σ_A is the applied stress; A is a variable related to the microstructure and is assumed to be a constant; n is the apparent stress exponent; Q is the apparent creep active energy; R is the universal gas constant; T is the absolute temperature. Besides, n and Q can be determined by increasing stress and temperature[43].

$$n = (\Delta \ln \varepsilon / \Delta \ln \sigma)_T \quad (3)$$

$$Q = kT^2(\Delta \ln \varepsilon / \Delta \ln T)_\sigma \quad (4)$$

According to the Eq. (2), the relationships between the strain rate during the steady-state creep stage and applied stress and temperature for this alloy are expressed as ($\ln\varepsilon$–$1/T$) and ($\ln\varepsilon$–$\ln\sigma$), as shown in Figs. 8(a) and (b), respectively. Substituting the strain rate of the steady-state creep stage in Fig. 5 into the calculation, it can be obtained that the apparent creep active energy (Q) and the apparent stress exponent (n) under conditions of 780–820 °C and 125–175 MPa are Q=274 kJ·mol^{-1} and n=1.96, respectively. The relationship between the apparent stress exponent and the creep mechanism of alloys is as follows[44]: (1) n=1, the main creep deformation mechanism is diffusion creep caused by directed migration of atoms and vacancies; (2) n=2, the main creep deformation mechanism is grain boundary sliding (GBS); (3) n=3, the climb rate of dislocations is higher than the slip rate, and the creep deformation rate is mainly controlled by the dislocation slip process; (4) n=4–7, the climb rate of dislocations is lower than the slip rate, and the creep deformation rate is mainly controlled by the climb process of dislocations; (5) n>7, the creep process of alloys is still mainly controlled by dislocation climb, but this situation mostly occurs in second phase particle strengthening materials.

According to the apparent stress exponent measured (n=1.96), it can be speculated that the sliding of the grain boundary dominates the creep strain rate during the steady-state creep stage. Lapin et al.[45] reported that the apparent stress exponent of a fully lamellar TiAl-based alloys under conditions of 700–800 °C and 200–400 MPa is about 5, which is higher than the Ti-46Al-8Nb alloy, indicating that the Ti-46Al-8Nb alloy exhibit better creep resistance within the temperature and stress range.

The creep deformation mechanism of the Ti-46Al-8Nb alloy under conditions of 780–820 °C and 125–175 MPa is dominated by grain boundary sliding (GBS), which requires the movement of dislocations to coordinate interface sliding and thereby enable creep deformation. Therefore, the dislocation density at the grain boundaries and interfaces between layers with different orientations should be significantly higher than that within the grains[46]. It is generally thought that the grain boundary sliding mechanism will increase the local internal stress at the boundary of a lamellar settlement[47]. With the help of externally applied creep stress, the dislocation sliding system of adjacent layer colony may be activated. As the applied stress increases, the number of dislocations in the alloy at grain boundaries and phase interfaces also increases. However, the triangular tangled grain boundary will slow down the grain boundary sliding mechanism[48]. The weakened grain boundary sliding requires large external creep stress to drive the activation of other dislocation slip systems.

4.3 Mechanism of crack initiation and propagation during creep

By analyzing the microstructure before and after creep

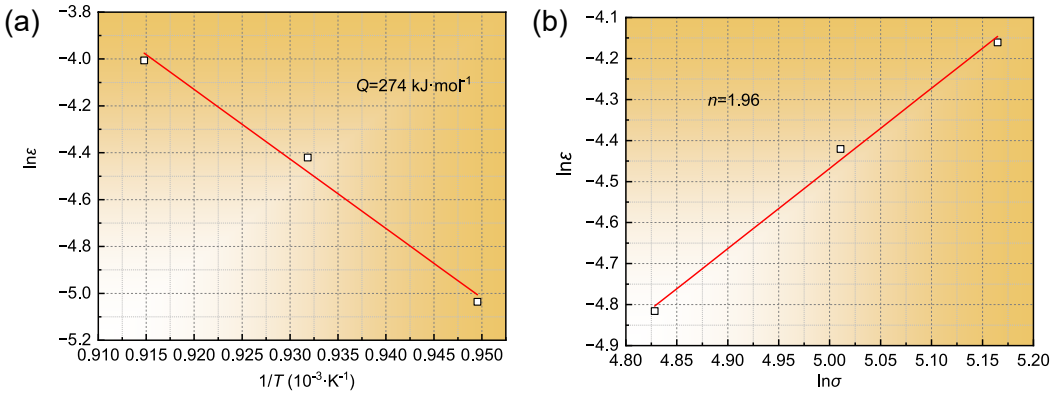

Fig. 8: Relationship between strain rate (ε) during steady-state creep stage and applied stress (σ), temperature (T) for the alloy: (a) strain rate and temperature; (b) strain rate and applied stress

performance testing, the schematic diagrams showing the nucleation and growth mechanism of cavities within the segregation zone are shown in Fig. 9. Cavities usually forms at the grain boundaries, caused by the presence of significant stress concentration and the low bonding strength at that location. As the creep goes on, the voids will continue to grow along the tensile direction and connect with each other to form larger voids, as shown in Figs. 9(b) and (c).

Figure 10 illustrates schematic diagrams of the microstructural evolution process during creep. The red dashed line marks the position of the grain boundary. Figures 10(a) and (c) show small and large block-like β segregation at the grain boundary, respectively. Whether it is β-segregation at grain boundaries or blocky γ+B2 phase within grains, the presence of voids in the segregation zone can lead to the instability of the alloy microstructure, which will result in complete dissolution of segregation during creep, as shown in Figs. 10(a) and (b). As the creep progresses, the smooth grain boundaries caused by small blocky β-segregation have a low hindering effect on the growth and connection of voids, ultimately leading to crack propagation at the grain boundaries and creep failure. Compared with small-blocky β-segregation, large-blocky β-segregation has a smaller specific surface area, which means a lower nucleation rate of voids. Therefore, due to the obstruction effect of irregular serrated grain boundaries caused by large-blocky β-segregation, cracks are difficult to propagate at the grain boundaries and can only form larger voids. When the accumulated energy in the alloy reaches a certain level, cracks will propagate along the interlayer of the grains until creep fracture occurs.

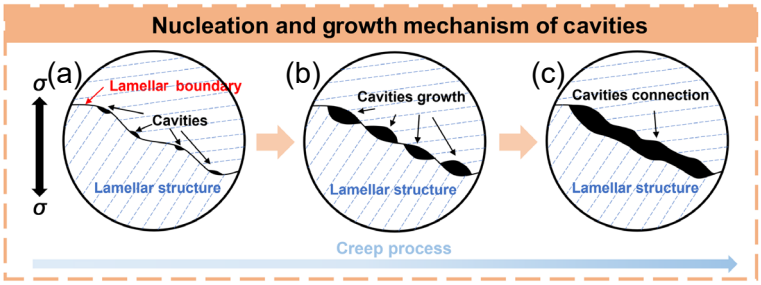

Fig. 9: Schematic diagrams showing nucleation and growth mechanism of cavities: (a) nucleation; (b) growth; (c) cavities interlink

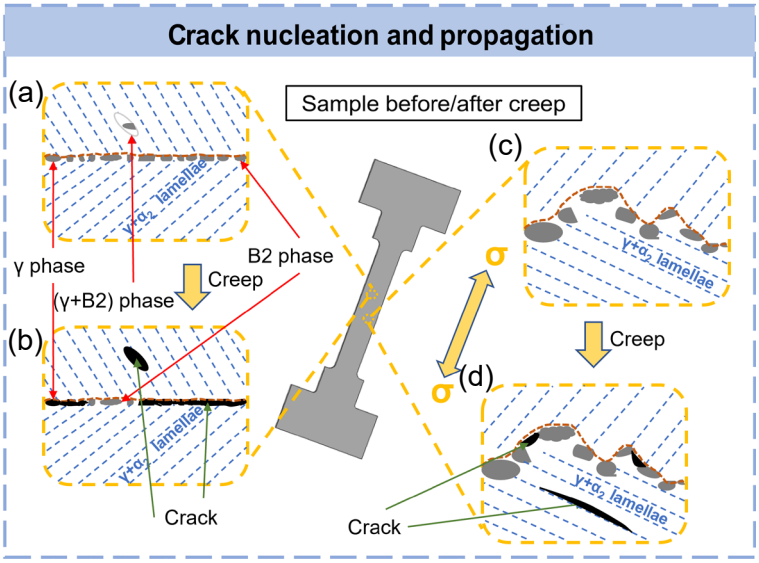

Fig. 10: Schematic diagrams showing microstructural evolution during creep: (a, b) small-block segregation smooth interface before (a) and after (b) creep testing; (c, d) large-block segregation irregular interface before (c) and after (d) creep testing

5 Conclusions

In this work, the Ti-46Al-8Nb alloy was prepared by electromagnetic cold crucible solidification technology, and the microstructure, phase constitution, creep performance, and creep deformation structure were studied. The following conclusions are obtained:

(1) The phase constitution of Ti-46Al-8Nb alloy consists of γ, α_2, and B2 phase. The alloy is composed of γ/α_2 lamellae with different orientations. Due to different micro-segregation degrees, there are two boundary morphologies, i.e., the smooth grain boundaries due to small-blocky segregation and irregular grain boundaries caused by large-blocky segregation.

(2) The solidification path of Ti-46Al-8Nb alloy transitions from single β solidification to hypoperitectic solidification. The growth of peritectic phase consumes residual liquid phase and primary β phase, resulting in a decrease in the amount of B2 phase formed by the ordering of β phase retained at room temperature, which is beneficial for improving creep resistance.

(3) The Ti-46Al-8Nb alloy exhibits typical creep characteristics, and there is an obvious steady-state creep stage. At 800 °C, as the applied stress increases, the steady-state creep rate of Ti-46Al-8Nb alloy increases from 0.0081%·h^{-1} to 0.0156%·h^{-1}. Under 150 MPa, when the temperature rises from 780 °C to 820 °C, the steady-state creep rate of Ti-46Al-8Nb alloy increases from 0.0065%·h^{-1} to 0.0182%·h^{-1}.

(4) The apparent creep active energy and the apparent stress exponent of the Ti-46Al-8Nb alloy is calculated to be Q=274 kJ·mol^{-1} and n=1.96 in the conditions of 780–820 °C and 125–175 MPa. The creep deformation mechanism of Ti-46Al-8Nb alloy is grain boundary sliding. The creep failure mechanism is that segregated areas dissolve to form voids, which grow and interconnect to promote crack propagation. For the smooth grain boundaries, cracks propagate along the grain boundaries; For the irregular serrated grain boundaries, cracks will propagate along the interlayer of the grains, ultimately leading to material failure.

(5) During the creep process, cracks in Ti-46Al-8Nb alloy usually initiate and propagate along the direction perpendicular to or at a 45° to the stress axis, until creep fracture occurs. Creep fracture is caused by the maximum tensile stress and shear stress in these two directions, respectively.

Acknowledgments

This work was supported by the National Natural Science Foundation of China (No. 52425401), the Foundation of National Key Laboratory for Precision Hot Processing of Metals (No. JCKYS2021603C001), the Fundamental Research Funds for the Central Universities (No. 2023FRFK06014), and the Major Science and Technology Achievement Transformation Project of Heilongjiang Province (No. ZC2023SH0075).

Conflict of interest

Prof. Rui-run Chen is an EBM of *CHINA FOUNDRY*. He was not involved in the peer-review or handling of the manuscript. The authors have no other competing interests to disclose.

References

[1] Liang W, Ma X X, Zhao X G, et al. Formation of siliconized layer on TiAl-based alloy and the oxidation resistance. Acta Metallurgica Sinica, 2003, 16(6): 466–472.
[2] Liu P, Hou B, Wang A Q, et al. Superior strength-plasticity synergy in a heterogeneous lamellar Ti_2AlC/TiAl composite with unique interfacial microstructure. Journal of Materials Science & Technology, 2023, 159: 21–32.
[3] Liu P, Wang Z B, Ye F, et al. Hierarchically heterogeneous strategy for Ti_2AlC/TiAl composite with superior mechanical properties. Composites, Part B-Engineering, 2024, 273: 111259.
[4] Hénaff G, Gloanec A L. Fatigue properties of TiAl alloys. Intermetallics, 2005, 13(5): 543–558.
[5] Lin J P, Xu X J, Wang Y L, et al. High temperature deformation behaviors of a high Nb containing TiAl alloy. Intermetallics, 2007, 15(5): 668–674.
[6] Ding X F, Lin J P, Zhang L Q, et al. Microstructural control of TiAl-Nb alloys by directional solidification. Acta Materialia, 2012, 60(2): 498–506.
[7] Janschek P. Wrought TiAl blades. Materials Today: Proceedings, 2015, 2: S92–S97.
[8] Reith M, Franke M, Schloffer M, et al. Processing 4th generation titanium aluminides via electron beam based additive manufacturing – characterization of microstructure and mechanical properties. Materialia, 2020, 14: 100902.
[9] Song L, Lin J, Li J. Effects of trace alloying elements on the phase transformation behaviors of ordered ω phases in high Nb-TiAl alloys. Materials & Design, 2017, 113: 47–53.
[10] Donald S, Kim Y. Sheet rolling and performance evaluation of beta gamma (β+γ) alloys. Ti-2007 Science and Engineering, Kyoto, Japan: The Japan Institute of Metals, 2007.
[11] Chen G, Sun Z, Zhou X. Oxidation and mechanical behavior of intermetallic alloys in the Ti-Nb-Al ternary system. Materials Science and Engineering: A, 1992, 153(1): 597–601.
[12] Yang G, Kou H, Yang J, et al. In-situ investigation on the β to α phase transformation in Ti-45Al-8.5Nb-(W, B, Y) alloy. Journal of Alloys and Compounds, 2016, 663: 594–600.
[13] Wang Q, Chen R R, Yang Y, et al. Effects of lamellar spacing on microstructural stability and creep properties in β-solidifying γ-TiAl alloy by directional solidification. Materials Science and Engineering: A, 2018, 711: 508–514.
[14] Trofimov D M, Imayev V M, Imayev R M. Preliminary study of the effect of Sn addition on microstructure and creep resistance of a β-solidifying TiAl alloy. Intermetallics, 2024, 169: 108310.
[15] Wang Q, Wu X, Bai Z, et al. Microstructures and mechanical properties of a γ-TiAl alloy modified by Gd additions. Materials Science and Engineering: A, 2024, 894: 146187.
[16] Zheng G, Tang B, Zhao S, et al. Evading the strength-ductility trade-off at room temperature and achieving ultrahigh plasticity at 800 °C in a TiAl alloy. Acta Materialia, 2022, 225: 117585.
[17] Erdely P, Staron P, Maawad E, et al. Design and control of microstructure and texture by thermomechanical processing of a multi-phase TiAl alloy. Materials & Design, 2017, 131: 286–296.
[18] Moon B M, Seo J H, Lee H J, et al. Method of recycling titanium scraps via the electromagnetic cold crucible technique coupled with calcium treatment. Journal of Alloys and Compounds, 2017, 727: 931–939.
[19] Su Y Q, Guo J J, Jia J, et al. Composition control of a TiAl melt during the induction skull melting (ISM) process. Journal of Alloys and Compounds, 2002, 334(1–2): 261–266.
[20] Niu H Z, Xiao S L, Kong F T, et al. Microstructure characterization and mechanical properties of TiB_2/TiAl in situ composite by induction skull melting process. Materials Science and Engineering: A, 2012, 532: 522–527.
[21] Guo J, Jia J, Liu Y, et al. Evaporation behavior of aluminum during the cold crucible induction skull melting of titanium aluminum alloys. Metallurgical and Materials Transactions: B, 2000, 31: 837–844.
[22] Ciszek T F. Growth and properties of [100] and [111] dislocation-free silicon crystals from a cold crucible. Journal of Crystal Growth, 1984, 70(1): 324–329.

[23] Elgamel H E, Ghannam M Y, Vinckier C, et al. Boosting the efficiency of solar cells fabricated on electromagnetic cold crucible cast multicrystalline silicon by means of hydrogen passivation. Solar Energy Materials and Solar Cells, 1994, 34(1): 237–241.
[24] Kassner M E, Pérez-Prado M T. Five-power-law creep in single phase metals and alloys. Progress in Materials Science, 2000, 45(1): 1–102.
[25] Sujata M, Sastry D H, Ramachandra C. Microstructural characterization and creep behaviour of as-cast titanium aluminide Ti-48Al-2V. Intermetallics, 2004, 12(7): 691–697.
[26] Kenel C, Leinenbach C. Influence of cooling rate on microstructure formation during rapid solidification of binary TiAl alloys. Journal of Alloys and Compounds, 2015, 637: 242–247.
[27] Liang Z, Xiao S, Shao Y, et al. Effects of tailoring microstructure on short-term creep behavior of high Nb containing TiAl alloys under various stress levels. Journal of Materials Research and Technology, 2023, 25: 532–545.
[28] Zhang T, Yuan H. Thermo-mechanical creep-fatigue damage evolution and life assessment of TiAl alloy. Materials Science and Engineering: A, 909: 146806.
[29] Loginov P A, Markov G M, Korotitskiy A V, et al. Compressive creep behavior of powder metallurgy manufactured Y_2O_3-reinforced TNM-B1 TiAl alloy with equiaxed and lamellar microstructure. Materials Characterization, 2023, 205: 113367.
[30] Wang Y, Xue X, Kou H, et al. Quasi-in-situ investigation on microstructure degradation of a fully lamellar TiAl alloy during creep. Journal of Materials Research and Technology, 2022, 18: 4980–4989.
[31] Chen G L, Xu X J, Teng Z K, et al. Microsegregation in high Nb containing TiAl alloy ingots beyond laboratory scale. Intermetallics, 2007, 15: 625–631.
[32] Schwaighofer E, Clemens H, Mayer S, et al. Microstructural design and mechanical properties of a cast and heat-treated intermetallic multi-phase γ-TiAl based alloy. Intermetallics, 2014, 44: 128–140.
[33] Zhu H, Wei T, Carr D, et al. Microstructural design for thermal creep and radiation damage resistance of titanium aluminide alloys for high-temperature nuclear structural applications. Current Opinion in Solid State and Materials Science, 2014, 18(5): 269–278.
[34] Abdallah Z, Ding R, Martin N, et al. Creep deformation mechanisms in a γ titanium aluminide. Materials Science and Engineering: A, 2016, 673: 616–623.
[35] Su Y Q, Liu C, Li X Z, et al. Microstructure selection during the directionally peritectic solidification of Ti-Al binary system. Intermetallics, 2005, 13(3–4): 267–74.
[36] Wu X H. Review of alloy and process development of TiAl alloys. Intermetallics, 2006, 14(10–11): 1114–1122.
[37] Johnson D R, Inui H, Muto S, et al. Microstructural development during directional solidification of α-seeded TiAl alloys. Acta Materialia, 2006, 54(4): 1077–1085.
[38] Li J, Song B, Nurly H, et al. Microstructure evolution and a new mechanism of B2 phase on room temperature mechanical properties of Ti-47Al-2Cr2Nb alloy prepared by hot isostatic pressing. Materials Characterization, 2018, 140: 64–71.
[39] Liang Z, Xiao S, Li Q, et al. Tensile creep behavior of a heat treated b-solidified g-TiAl alloy: the development of dynamic recrystallization and the role of B2 phase. Materials Science and Engineering: A, 2023, 863: 144522.
[40] Tian S, Wang Q, Yu H, et al. Microstructure and creep behaviors of a high Nb-TiAl intermetallic compound based alloy. Materials Science and Engineering: A, 2014, 614: 338–346.
[41] Sherby O D, Orr R L, Dorn J E. Creep correlations of metals at elevated temperatures. JOM, 1954, 6: 71–80.
[42] Barrett C, Ardell A, Sherby O. Influence of modulus on the temperature dependence of the activation energy for creep at high temperatures. Transactions of the Metallurgical Society of AIME, 1964, 230: 200–204.
[43] Evans A, Rawlings R. The thermally activated deformation of crystalline materials. Physica Status Solidi: B, 1969, 34(1): 9–31.
[44] Wang J N, Schwartz A J, Nieh T G, et al. Reduction of primary creep in TiAl alloys by prestraining. Materials Science and Engineering: A, 1996, 206(1): 63–70.
[45] Lapin J, Pelachová T, Dománková, M. Creep behaviour of a new air-hardenable intermetallic Ti-46Al-8Ta alloy. Intermetallics, 2011, 19: 814–8193.
[46] Beddoes J, Triantafillou J, Zhao L. Effect of stress on creep of lamellar near γ-TiAl. MRS Online Proceedings Library (OPL), 1996, 460: 293.
[47] Guo Y, Xiao S, Tian J, et al. The influence of stress levels on the creep behavior of Ti-42Al6Nb-0.05Y_2O_3 alloy. Journal of Materials Research and Technology, 2022, 20: 269–80.
[48] Wang Q, Chen R R, Yang Y H, et al. Effects of V and B, Y additions on the microstructure and creep behaviour of high-Nb TiAl alloys. Journal of Alloys and Compounds, 2018, 747: 640–647.